

Ripplocations in Layered Materials: Sublinear Scaling and Basal Climb

James G. McHugh,* Pavlos Mouratidis, and Kenny Jolley

*Dept. of Chemistry, Loughborough University
Epinal Way, Loughborough LE11 3TU, United Kingdom*

(Dated: December 22, 2024)

The *ripplocation* is a crystallographic defect which is unique to layered materials, combining nanoscale delamination with the crystallographic slip of a basal dislocation. Here, we have studied basal dislocations and ripplocations using analytical and computational techniques. Expressions for the energetic and structural scaling factors of surface ripplocations are derived, which are in close correspondence to the physics of a classical carpet ruck. Our simulations demonstrate that the lowest-energy structure of dislocation pile-ups in layered materials is the ripplocation, while large dislocation pile-ups in bulk graphite demonstrate multilayer delamination, curvature and voids. This can provide a concise explanation for the large volumetric expansion seen in irradiated graphite.

Introduction. — It has long been understood that the plastic deformation of solids proceeds primarily through the nucleation of linear defects, called dislocations, which locally accommodate crystallographic slip. The slipped and unslipped crystal regions on either side of a dislocation line are related through translation by a lattice vector, which is a topological property of that dislocation, called its *Burgers vector*, \mathbf{b} . The dynamics of dislocations are dominated by Frank’s rule, which dictates that the energy of a dislocation is quadratic in the Burgers vector, $E \propto \mathbf{b}^2$. This causes perfect dislocations to dissociate into partials, with Burgers vector of less than a full lattice translation [1–3].

Recently, distinct behaviour has been observed in layered materials. Surface ripples with well-defined crystallographic character comprising sharp, localised folds between regions which are slipped relative to one another by an in-plane lattice vector have been observed at the (0001) surface of exfoliated MoS₂ samples and graphite nanoplatelets [4, 5]. These defects combine the properties of edge dislocations and delamination, and have been termed *ripplocations*. Extensive spherical nanoindentation experiments have demonstrated that the deformation behaviour of a wide variety of layered materials proceeds not through the basal dislocation, but through a distinct and reversible mechanism, which has been attributed to the formation of ripplocations [6]. Ripplocations are now believed to occur on a variety of length scales, accounting for material deformation in substances as diverse as playing cards and steel sheets to phyllosilicates in the lithosphere [7–9].

In contrast to the classical dislocation, ripplocations exhibit a *sublinear* energy scaling as a function of Burgers vector, $E \propto \mathbf{b}^\beta$, where $\beta < 1$. This ensures that ripplocations comprised of multiple Burgers vector become increasingly energetically favourable as a function of extra material, as $|\mathbf{b}_1 + \mathbf{b}_2|^\beta < |\mathbf{b}_1|^\beta + |\mathbf{b}_2|^\beta$. While this sublinearity has been well-established, there is reasonable variation in the literature with reported values lying in

the range $\beta \approx 0.3 - 0.45$ [4, 10, 11]. Additionally, while there have been computational studies of ripplocations, no rigorous comparison has been made between them and the corresponding dislocation cores.

In this work, we have applied analytical and computational techniques which accurately model the interlayer friction between van der Waals layers to calculate the energetic and structural scaling factors of surface and bulk ripplocations. In van der Waals materials the interlayer friction is encapsulated in the γ -surface energy to slide adjacent layers along different crystallographic directions [12–15]. This is essential in accurately modelling these defects, as it is the resistance to sliding against adjacent layers that stabilises basal dislocations & ripplocations (for additional details see Fig. S1-S2). Our simulations of dislocation pile-ups in large systems demonstrate that the locally buckled ripplocation structure is the preferred mode of deformation with increasing additional material in the pile-up.

Methods. — Density Functional Theory (DFT) calculations have been performed using plane-wave basis Kohn Sham states as implemented in the Quantum Espresso package [16, 17]. We have employed Vanderbilt ultrasoft pseudopotentials [18] with cut-offs of $E_{cut} = 40$ Ry. A Γ -centred $1 \times 5 \times 1$ k -point grid is found to sample the Brillouin zone with sufficient accuracy, giving total energy convergence to within 0.1 meV/atom for all structures. Molecular dynamics (MD) simulations have been performed in LAMMPS [19], using the hybrid neural network (hNN) potential for multilayer graphene systems developed by Wen and Tadmor, which we have benchmarked against DFT and other interlayer potentials [20, 21].

Surface ripplocations. — Surface ripplocations have been created through the insertion of additional rows of material to the top layer of a bilayer structure in a periodic ribbon geometry, which is extended along one crystallographic orientation. Atoms in the top layer are allowed to fully relax, while the bottom layer is held fixed by setting all forces to zero, to approximate a compressed monolayer on a substrate. This approach has been verified in comparison to a fully-relaxed, multilayer graphite substrate using MD calculations (for more details see Fig.

* j.g.mchugh@lboro.ac.uk

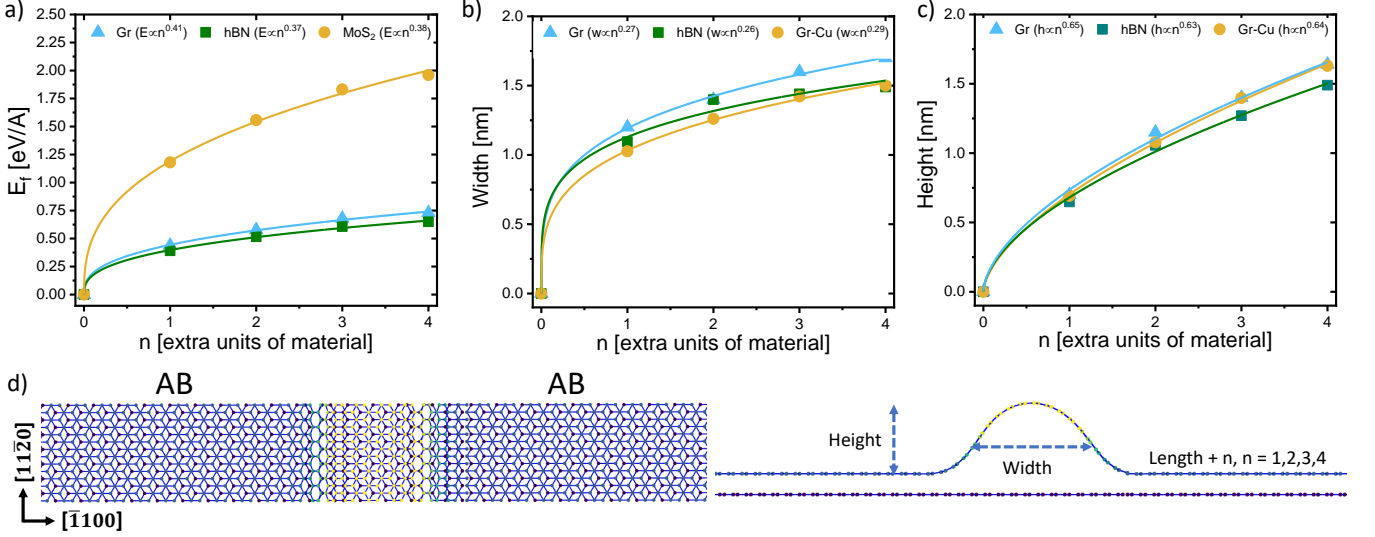


FIG. 1. (a) Formation energy of epitaxial graphene, MoS₂ and hBN sheets vs amount of additional material n . (b) Width and (c) Height of epitaxial graphene on graphene, hBN on hBN and graphene on the Cu(100) surface (d) Schematic depiction of ripplocation configuration and associated structural properties.

S3-S4).

The amount of additional material is quantified using the parameter n , denoting a Burgers vector of multiple lattice translations. Along the zigzag direction this corresponds to an edge dislocation ($n = 1$) or superdislocation ($n > 1$), $\mathbf{b}_{zz} = n \times [1\bar{2}10]$. Along the armchair direction $\mathbf{b}_{ac} = n \times [\bar{1}100]$, and all edge dislocations are superdislocations. Thus, n quantifies the number of edge dislocations in the superdislocation pile-up, and is the characteristic property of a ripplocation defect.

DFT structural relaxations have been performed for zigzag surface ripplocations, $\mathbf{b} = n \times [1\bar{2}10]$ in graphene, hexagonal boron nitride (hBN) and MoS₂. While the initial configuration is that of a superdislocation, with a well-defined Burgers vector, upon relaxation the large initial in-plane strains are released by out of plane buckling. This gives close to equilibrium bond lengths across the ripplocation (see Fig. S5-S6), and prior work has suggested that ripplocations do not possess a long range Burgers vector [4, 10].

Formation energies E_f are calculated from the optimised cells as:

$$E_f = E_{cell} - N\epsilon_{BL}, \quad (1)$$

where E_{cell} is the energy of a defected bilayer, ϵ_{BL} is the energy per atom of a perfect bilayer, and N is the number of atoms. The height has been calculated as the distance between the flat top layer and the ripple's peak. The width has been calculated as the FWHM, as is shown schematically in Fig. 1(d). The formation energy as a function of n is shown in Fig. 1(a) for all three materials, where we observe the expected sublinear dependence on \mathbf{b} , with similar scaling factors in the range $\beta \approx 0.37 - 0.41$.

Scaling relations. — The universality of the observed

scaling law warrants further consideration. Taking the above consideration of the unstrained bond length into account, we may model the ripplocation as a ruck in an inextensible material [22, 23]. We then consider two energetic contributions to the core energy,

$$E(w) = U_e(w) + U_s(w) = B\kappa^2 w + Vth^\alpha w. \quad (2)$$

The relevant energy terms comprise the elastic energy U_e and the adhesion energy U_s , which is the energy acquired from the shifting and out of plane deformation across a ripple. The elastic energy is taken simply as $U_e = B\kappa^2 w$ where B is the *elastic bending energy*, w is the width and κ is the net curvature across a ripple. The interfacial term encapsulates the adhesion energy across the core, which we take to be $Vth^\alpha w$ where V is the interlayer adhesion energy of the absorbed layer to the substrate, h is the height of the ruck and t is the monolayer thickness.

The most important modification of this expression with respect to the classical equation for an inextensible ruck is the incorporation of the sublinearity factor α , which accounts for the deviation from classical behaviour for van der Waals layers. We note that when $\alpha = 1$ this corresponds to the classical rucking of a sheet under the influence of gravity. We solve for the equilibrium width by considering the derivative of the energy equation (1) with respect to the defect width,

$$\frac{dE(w)}{dw} = -\frac{2Eb}{w^3} + tV(bw)^{\alpha/2} w = 0, \quad (3)$$

where we make use of the relations $h = \sqrt{bw}$ and $\kappa = \frac{h}{w^2}$ for the arc-length and curvature of a clamped elastica.

The ruck energy as a function of width is then,

$$E(w) = (B + tV)A(\alpha) \frac{2+\alpha}{6+\alpha} b^{1-(4-2\alpha)/(6+\alpha)} \quad (4)$$

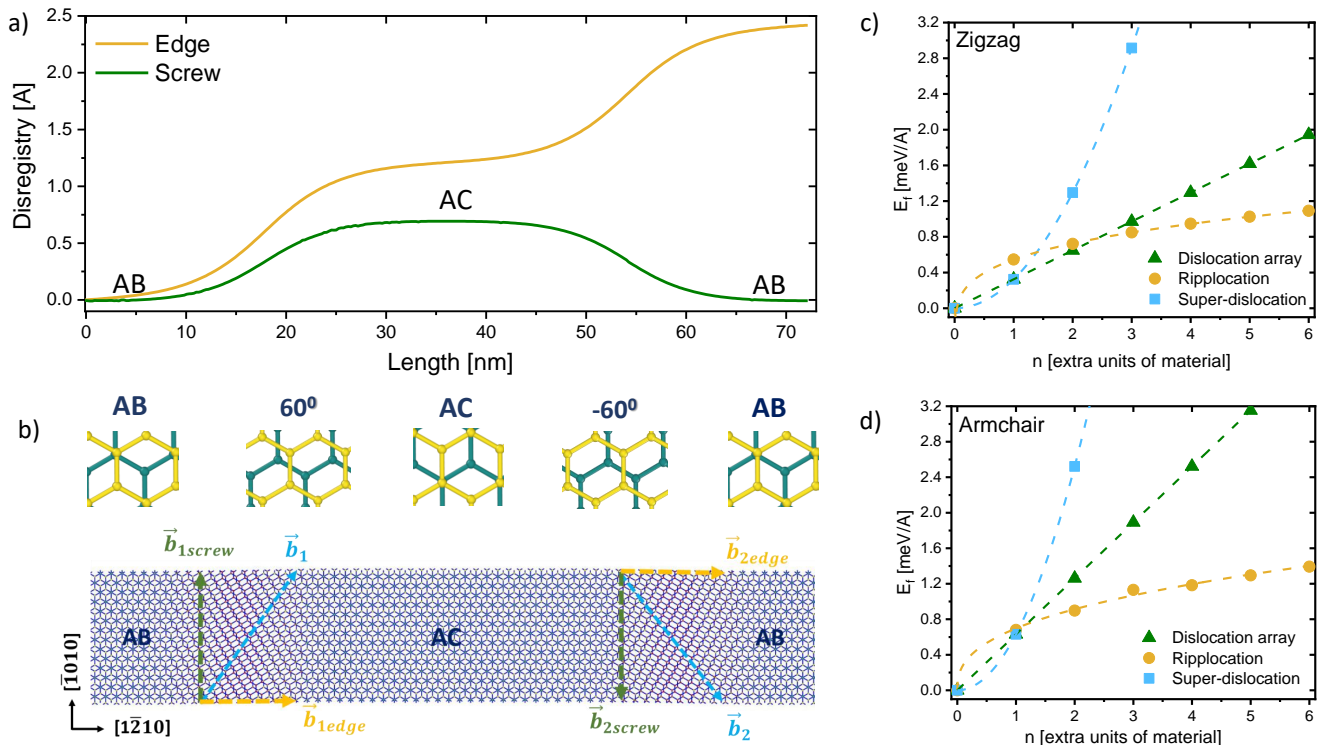


FIG. 2. (a) Disregistry vs length and (b) cell configuration and local stacking in a dislocated bilayer (c) Comparison of superdislocation, dislocation array and ripplcation energies for Burgers vectors along to the zigzag and (d) armchair directions.

Method	α	$E \propto b^{\beta(\alpha)}$	$w \propto b^{\gamma(\alpha)}$	$h \propto b^{\delta(\alpha)}$
Theoretical	0.166	0.405	0.262	0.648
Gr (DFT)	0.177	0.410	0.271	0.650
Gr (hNN)	0.100	0.377	0.253	0.612
hBN (DFT)	0.081	0.369	0.261	0.631
MoS ₂ (DFT)	0.102	0.378	0.287	0.610

TABLE I. Energy, width, height scalings for different computational methods.

Consequently, taking a value of $\alpha = 1/6$, we find that $E(b) \propto b^{\beta(\alpha)}$ where,

$$\beta(\alpha) = 1 - \frac{4 - 2\alpha}{6 + \alpha} = 1 - \frac{22}{37} = \frac{15}{37} \approx 0.41 \quad (5)$$

This sublinear scaling as a function of height can be understood as a consequence of the van der Waals interaction, which scales as a function of distance as r^{-6} , here incorporated through the sublinearity factor α . This immediately leads to the fact that material closer to the substrate matters proportionally much more than that which is further away, so that the overall energy scales very slowly in the maximum height.

These considerations also immediately lead to scalings for the height and width as $w(b) \propto b^{\gamma(\alpha)}$ and $h(b) \propto b^{\delta(\alpha)}$, which are in exceptionally good agreement (see Table 1) with our first-principles simulations. Additionally, since we have only considered the bending and adhesion en-

ergies, this scaling behaviour is immediately applicable to physisorbed monolayers on other substrates, and our DFT simulation of the graphene/Cu(100) surface interaction (see Fig. S7-S8), again agree closely to the analytical results as shown in Fig. 1(b) and 1(c).

Basal Dislocations — Having precisely established the energetic and structural scaling of surface ripplcations, we now compare the corresponding properties of basal dislocations. The basal dislocation core in graphite and other layered materials is wide (>10 nm) [24–26] due to the weak interlayer interactions, and therefore difficult to simulate via DFT [27, 28]. To address this, we have conducted simulations of large defected bilayer cells of up to 500 nm in length, using the hNN potential [15].

To validate this potential and compare to DFT, we performed relaxation of surface ripplcations for increasing n , along both armchair and zigzag directions. Our results for the energetic and structural scaling factors using the hNN potential are consistent with DFT, as are all other potentials which include an accurate interlayer term. Potentials which do not correctly capture the γ -surface energy, give inconsistent results and with increasing cell length ripples become wider and lower until they eventually lie completely flat. A full comparison of different potentials is given in Supplemental Information, Fig. S9-S10.

It can be seen in Fig. 2(c) and Fig. 2(d) that at small n , for Burgers vector along both crystallographic

directions, the lowest-energy structures are not localised ripples, but rather arrays of partial dislocations with net Burgers vector equal to the initial superdislocation Burgers vector, Fig. 2(a) and Fig. 2. (b). For the zigzag core this gives pairs of $\pm 60^\circ$ partials, $\mathbf{b}_{zz} = n \times 1/3[12\bar{1}0] = n \times (1/3[1\bar{1}00] + 1/3[0\bar{1}10])$ for $n < 3$, above which ripplocations are nucleated in preference to dislocation arrays. Along the armchair direction, the initial $n = 1$ superdislocation dissociates into a sequence of four partial dislocations, a pair of $\pm 30^\circ$ partials and a pair of edge partials, $\mathbf{b}_{ac} = n \times \sqrt{3}[10\bar{1}0] = n \times (\sqrt{3}/6[1\bar{1}00] + \sqrt{3}/6[01\bar{1}0] + \sqrt{3}/3[10\bar{1}0] + \sqrt{3}/3[10\bar{1}0])$, and ripplocations are preferred for $n > 1$. This behaviour is again consistent with that of a ruck in a classical inextensible material, where under an initial compression, a sheet will not buckle unless the ratio of the initial compression to the coefficient of static friction of the substrate interaction, here encapsulated in the γ -surface, is above a critical value [22].

Two-dimensional ripples. — MD simulations also permit calculations of larger structures, such as the two-dimensional ripplocation junction shown in Fig. 3 (some additional structures are shown in Fig. S11) This has been created by inserting material along both the armchair and zigzag directions on the surface of a bilayer cell. A number of these structures have been simulated and in all cases we find highly sublinear scaling of the surface energy as a function of additional material, similar to the one-dimensional defects (Fig. S12). The pictured cell, which has an initial Burgers vector $\mathbf{b} = (b_{ac}, b_{zz}) = (2, 1)$, results in the formation of a ripplocation junction, where perpendicular dislocation lines meet at an AA-stacked core. It is noteworthy that this type of structure is strikingly similar to experimental transmission electron microscopy (TEM) images of irradiated highly oriented pyrolytic graphite (HOPG) surfaces [29, 30], and in this context our large-scale simulations provide further evidence of dislocation pile-up as the likely deformation mode of irradiated HOPG. We leave further, systematic investigation of these two-dimensional defects to future work.

Bulk. — We now discuss the behaviour of bulk ripplocations in large MD cells. Cells containing bulk ripplocations are created similarly to surface ripplocations, where extra rows of material are inserted into a monolayer in a bulk cell. For small n , this again gives dislocation arrays and a linear energy dependence. Above a critical value of n , the formation energy is almost constant with additional material as shown in Fig. 4(b), and the folded-over bulk ripplocation, or "ruck & tuck" structure is nucleated [31]. Notably, the surrounding sheets have the lowest-energy Bernal stacking (see Fig. S13) and we conclude that slip of the folded defect into the surrounding layer is inhibited due to friction.

The constant formation energy can be understood with reference to the relaxed structures, shown in Fig. 4(a). As extra material is added, it is accommodated by increasing the length of the prismatic sheet bounded by

the highly curved regions, while the curved regions remain approximately the same. This demonstrates that for both bulk and surface ripples, curvature can essentially be seen as the mechanism of dislocation climb for basal dislocations in layered materials. This proceeds unconstrained on the surface, while in bulk additional material is accommodated simply by growing the flat, perfectly-stacked prismatic layer.

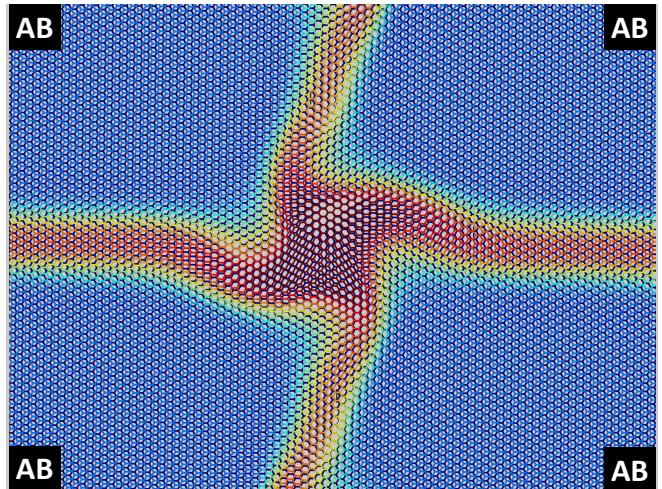


FIG. 3. Two-dimensional surface ripplocation junction.

Dislocation pile-ups on multiple adjacent layers in bulk graphite have also been considered, through the incorporation of extra material to a number of adjacent layers in a large bulk simulation cell. Upon relaxation, this results in an even lower energy per Burgers vector per layer than the single-layer ruck and tuck, Fig. 4(d). This also gives distinct structures, which are similar to bulk twin boundaries [32], demonstrating multilayer curvature and the formation of voids adjacent to the compressed region, a representative structure is shown in Fig. 4(c) (some additional structures for pile-ups of different Burgers vector and number of layers, are shown in Fig. S14). The ruck and tuck can then be seen as a limiting case where compression occurs on only one layer. Furthermore, all such structures essentially demonstrate basal climb, i.e., c-axis expansion to release in-plane compression.

Discussion. — The application of classical mechanics to the nanoscale buckling of two-dimensional monolayers has typically proven difficult. In this work, we have found that minor modification of classical expressions gives exceptional agreement to DFT calculations. The energy scaling, Eq. 2, is based only on classical expressions for clamped elastica and is, therefore, directly applicable to any inextensible layered material, through simple modification of the α sublinearity parameter. This reinforces the idea that ripplocations are a general concept applicable at a variety of length-scales, since we have considered only monolayer bending and adhesion.

The exceptionally low sublinear factor, $\alpha \approx 0.1$, in comparison to a sheet under the influence of gravity, ex-

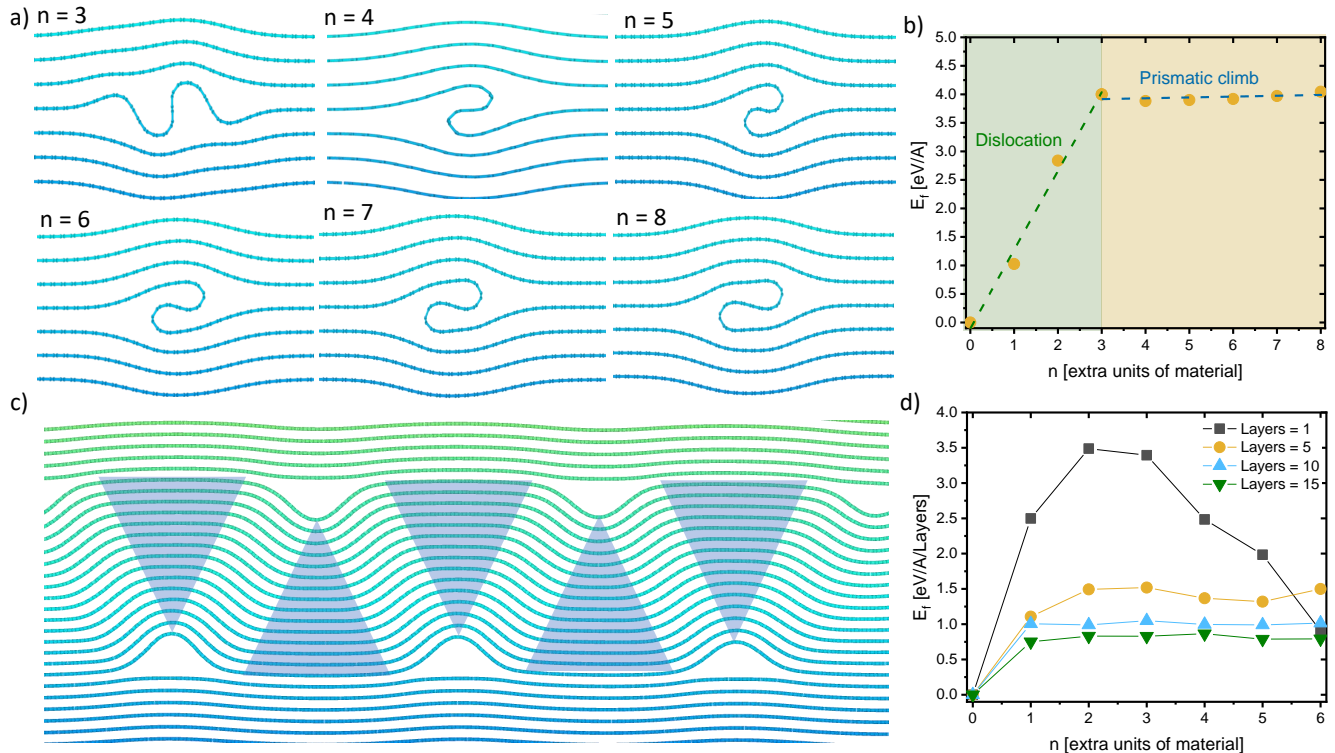


FIG. 4. (a) Ruck and tuck structures (b) energy vs extra material, n , for the single-layer pileup. (c) Multilayer dislocation pile-up (d) Energy per Burgers vector of multilayer dislocation pile-ups.

plains the exaggerated tendency of epitaxial monolayers to wrinkle and ripple. Our work therefore indicates that the most important property in the wrinkling of epitaxially-grown monolayers is the coefficient of friction between the monolayer and the substrate. This can explain, for example, the high density of wrinkle formation in graphene adsorbed on the highly incommensurate Cu(100) and Cu(110) surfaces [33] in comparison to the almost-commensurate Cu(111) face. It is therefore noteworthy that the ripplation formation energy is close to the observed experimental energy barrier for wrinkle nucleation on Ir(100) substrates. [34, 35]

In all cases, buckling of the ripplation can be seen as a type of climb mechanism for basal dislocations. Our work therefore has important implications for the irradiation-induced deformation of HOPG. Under irradiation, HOPG and even single graphene sheets will shrink, which very quickly leads to the formation of basal dislocations. The very low Peierls barrier in layered materials ensures that the basal dislocation core is very diffuse and easy to move, which readily allows dislocation pile-ups [28, 31]. Under this compression, our work confirms that these dislocation pile-ups will result in delaminated, curved regions of microstructure rather than flat superdislocation cores. This suggests that essentially a process of sub-surface wrinkling is implicated in the pronounced

c -axis expansion of irradiated HOPG samples, with increasing compression resulting in the formation of ripplation arrays, voids, ruck and tucks and highly curved regions. It is then unsurprising that there are substantial similarities between our simulations and experiment. Under heavy ion bombardment, in-plane dislocations are nucleated, which evolve into rippled "kink boundaries". These two-dimensional dislocation complexes are almost identical to our simulations of surface ripplation arrays, Fig. 3. There is also substantial experimental evidence for the formation of the single-layer ruck & tuck in irradiated graphite, [8, 36–41]. In addition, our multilayer simulations are similar to the regions of curvature and voids, which have recently been found in irradiated HOPG [42], again demonstrating damage due to compression and pile-up. In sum, this correspondence implicates the compression-induced dislocation pile-up and rippling of graphene monolayers as a concise and appealing explanation of the irradiation-induced deformation of single crystal graphite.

Acknowledgments — JGM was supported by the UK EPSRC grant EP/R005745/1. KJ and PM gratefully acknowledge funding from EDF Energy. The authors acknowledge the use of the HPCMidlands+ facility, funded by EPSRC grant EP/P020232/1.

- [1] F. C. Frank and J. H. van der Merwe. *Proceedings of the Royal Society of London. Series A. Mathematical and Physical Sciences*, 198(1053):205–216, August 1949.
- [2] F. C. Frank and W. T. Read. *Physical Review*, 79(4):722–723, August 1950.
- [3] F.C. Frank. *The London, Edinburgh, and Dublin Philosophical Magazine and Journal of Science*, 42(331):809–819, August 1951.
- [4] Akihiro Kushima, Xiaofeng Qian, Peng Zhao, Sulin Zhang, and Ju Li. *Nano Letters*, 15(2):1302–1308, January 2015.
- [5] A.V. Alaferdov, R. Savu, M.A. Canesqui, Y.V. Kopelevich, R.R. da Silva, N.N. Rozhkova, D.A. Pavlov, Yu.V. Usov, G.M. de Trindade, and S.A. Moshkalev. *Carbon*, 129:826–829, April 2018.
- [6] M.W. Barsoum and G.J. Tucker. *Scripta Materialia*, 139:166–172, October 2017.
- [7] Joe Aslin, Elisabetta Mariani, Karl Dawson, and Michel W. Barsoum. *Nature Communications*, 10(1), February 2019.
- [8] Michel W. Barsoum. *Frontiers in Materials*, 7, May 2020.
- [9] M. W. Barsoum, X. Zhao, S. Shanazarov, A. Romanchuk, S. Koumlis, S. J. Pagano, L. Lamberson, and G. J. Tucker. Rippllocations: A universal deformation mechanism in layered solids. *Physical Review Materials*, 3(1), January 2019.
- [10] Jacob Gruber, Andrew C. Lang, Justin Griggs, Mitra L. Taheri, Garritt J. Tucker, and Michel W. Barsoum. *Scientific Reports*, 6(1), September 2016.
- [11] Alireza Ostadhosseini, Ali Rahnamoun, Yuanxi Wang, Peng Zhao, Sulin Zhang, Vincent H. Crespi, and Adri C. T. van Duin. *The Journal of Physical Chemistry Letters*, 8(3):631–640, January 2017.
- [12] Shuyang Dai, Yang Xiang, and David J. Srolovitz. *Physical Review B*, 93(8), February 2016.
- [13] Aleksey N. Kolmogorov and Vincent H. Crespi. *Physical Review B*, 71(23), June 2005.
- [14] Andrey M. Popov, Irina V. Lebedeva, Andrey A. Knizhnik, Yurii E. Lozovik, and Boris V. Potapkin. *Physical Review B*, 84(24), December 2011.
- [15] Mingjian Wen, Stephen Carr, Shiang Fang, Efthimios Kaxiras, and Ellad B. Tadmor. *Physical Review B*, 98(23), December 2018.
- [16] Giannozzi et. al. *Journal of Physics: Condensed Matter*, 21(39):395502, Sep 2009.
- [17] Giannozzi et. al. *Journal of Physics: Condensed Matter*, 29(46):465901, Oct 2017.
- [18] Kevin F. Garrity, Joseph W. Bennett, Karin M. Rabe, and David Vanderbilt. *Computational Materials Science*, 81:446–452, January 2014.
- [19] Steve Plimpton. *Journal of Computational Physics*, 117(1):1–19, March 1995.
- [20] E. B. Tadmor, R. S. Elliott, J. P. Sethna, R. E. Miller, and C. A. Becker. *JOM*, 63(7):17–17, July 2011.
- [21] Ryan S. Elliott and Ellad B. Tadmor, 2011.
- [22] Dominic Vella, Arezki Boudaoud, and Mokhtar Adda-Bedia. *Physical Review Letters*, 103(17), October 2009.
- [23] John M. Kolinski, Pascale Aussillous, and L. Mahadevan. *Physical Review Letters*, 103(17), October 2009.
- [24] J. S. Alden, A. W. Tsen, P. Y. Huang, R. Hovden, L. Brown, J. Park, D. A. Muller, and P. L. McEuen. *Proceedings of the National Academy of Sciences*, 110(28):11256–11260, June 2013.
- [25] Junhao Lin, Wenjing Fang, Wu Zhou, Andrew R. Lupini, Juan Carlos Idrobo, Jing Kong, Stephen J. Pennycook, and Sokrates T. Pantelides. *Nano Letters*, 13(7):3262–3268, June 2013.
- [26] Benjamin Butz, Christian Dolle, Florian Niekiel, Konstantin Weber, Daniel Waldmann, Heiko B. Weber, Bernd Meyer, and Erdmann Spiecker. *Nature*, 505(7484):533–537, December 2013.
- [27] Irina V. Lebedeva, Alexander V. Lebedev, Andrey M. Popov, and Andrey A. Knizhnik. Dislocations in stacking and commensurate-incommensurate phase transition in bilayer graphene and hexagonal boron nitride. *Physical Review B*, 93(23), June 2016.
- [28] Rob H. Telling and Malcolm I. Heggie. *Philosophical Magazine Letters*, 83(7):411–421, July 2003.
- [29] J.A. Hinks, S.J. Haigh, G. Greaves, F. Sweeney, C.T. Pan, R.J. Young, and S.E. Donnelly. Dynamic microstructural evolution of graphite under displacing irradiation. *Carbon*, 68:273–284, March 2014.
- [30] Jonathan A. Hinks, G. Greaves, Sarah J. Haigh, Cheng-Ta Pan, and Stephen E. Donnelly. Kink band formation in graphite under ion irradiation at 100 and 298 k. *MATERIALS TRANSACTIONS*, 55(3):447–450, 2014.
- [31] M.I. Heggie, I. Suarez-Martinez, C. Davidson, and G. Haffenden. *Journal of Nuclear Materials*, 413(3):150–155, June 2011.
- [32] A. P. Rooney, Z. Li, W. Zhao, A. Gholinia, A. Kozikov, G. Auton, F. Ding, R. V. Gorbachev, R. J. Young, and S. J. Haigh. Anomalous twin boundaries in two dimensional materials. *Nature Communications*, 9(1), September 2018.
- [33] Bing Deng, Zhenqian Pang, Shulin Chen, Xin Li, Caixia Meng, Jiayu Li, Mengxi Liu, Juanxia Wu, Yue Qi, Wenhui Dang, Hao Yang, Yanfeng Zhang, Jin Zhang, Ning Kang, Hongqi Xu, Qiang Fu, Xiaohui Qiu, Peng Gao, Yujie Wei, Zhongfan Liu, and Hailin Peng. Wrinkle-free single-crystal graphene wafer grown on strain-engineered substrates. *ACS Nano*, 11(12):12337–12345, December 2017.
- [34] Hichem Hattab, Alpha T. N’Diaye, Dirk Wall, Claudius Klein, Giriraj Jnawali, Johann Coraux, Carsten Busse, Raoul van Gastel, Bene Poelsema, Thomas Michely, Frank-J. Meyer zu Heringdorf, and Michael Horn von Hoegen. *Nano Letters*, 12(2):678–682, January 2012.
- [35] Alpha T NDiaye, Raoul van Gastel, Antonio J Martínez-Galera, Johann Coraux, Hichem Hattab, Dirk Wall, Frank-J Meyer zu Heringdorf, Michael Horn von Hoegen, José M Gómez-Rodríguez, Bene Poelsema, Carsten Busse, and Thomas Michely. In situ observation of stress relaxation in epitaxial graphene. *New Journal of Physics*, 11(11):113056, November 2009.
- [36] Anjana Asthana, Yoshio Matsui, Makoto Yasuda, Koji Kimoto, Tadao Iwata, and Ken ichi Ohshima. *Journal of Applied Crystallography*, 38(2):361–367, March 2005.
- [37] J. Eapen, R. Krishna, T. D. Burchell, and K. L. Murty. *Materials Research Letters*, 2(1):43–50, November 2013.
- [38] S. Muto and T. Tanabe. *Journal of Electron Microscopy*, 48(5):519–523, January 1999.
- [39] Steve Johns, Lingfeng He, Karen Bustillo, William E.

- Windes, Rick Ubic, and Chinnathambi Karthik. *Carbon*, 166:113–122, September 2020.
- [40] Steve Johns, Lingfeng He, Joshua J. Kane, William E. Windes, Rick Ubic, and Chinnathambi Karthik. Experimental evidence for ‘buckle, ruck and tuck’ in neutron irradiated graphite. *Carbon*, 159:119–121, April 2020.
- [41] C.-T. Pan, J. A. Hinks, Q. M. Ramasse, G. Greaves, U. Bangert, S. E. Donnelly, and S. J. Haigh. *Scientific Reports*, 4(1), October 2014.
- [42] Steve Johns, Tyler Poulsen, Joshua J. Kane, William E. Windes, Rick Ubic, and Chinnathambi Karthik. Formation of carbon nanostructures in nuclear graphite under high-temperature in situ electron-irradiation. *Carbon*, 143:908–914, March 2019.
- [43] Fangyuan Zheng, Quoc Huy Thi, Lok Wing Wong, Qingming Deng, Thuc Hue Ly, and Jiong Zhao. *ACS Nano*, 14(2):2137–2144, January 2020.
- [44] Levente Tapasztó, Traian Dumitrică, Sung Jin Kim, Péter Nemes-Incze, Chanyong Hwang, and László P. Biró. *Nature Physics*, 8(10):739–742, August 2012.
- [45] Wenzhong Bao, Feng Miao, Zhen Chen, Hang Zhang, Wanyoung Jang, Chris Dames, and Chun Ning Lau. *Nature Nanotechnology*, 4(9):562–566, July 2009.
- [46] Shikai Deng and Vikas Berry. *Materials Today*, 19(4):197–212, May 2016.
- [47] Oded Hod. In *Handbook of Materials Modeling*, pages 1–25. Springer International Publishing, 2018.
- [48] Mingjian Wen and Ellad B. Tadmor. Hybrid neural network potential for multilayer graphene. *Physical Review B*, 100(19), November 2019.